

# Single-Crystal Organic Field-Effect Transistors Based on 5,15-Bisaryl-Tetrabenzoporphyrins: Synthesis, Structure, and Charge Transport Properties

Kazuya Miyazaki, Kento Teranishi, Hiroshi Matsuda, Kyohei Matsuo, Mitsuaki Yamauchi, Yoshiyuki Mizuhata, Nobutaka Shioya, Takeshi Hasegawa, and Hiroko Yamada\*

Dedicated to Women in emerging organic and hybrid electronic materials and interfaces

This study reports the fabrication and performance of single-crystal organic field-effect transistors (SC-OFETs) based on three 5,15-bisaryl-tetrabenzoporphyrin (BP) derivatives: C8Ph-BP, C8Ph-Ph-BP, and Ph-BP, where C8Ph and Ph are 4-*n*-octylphenyl and phenyl groups, respectively. These compounds are designed to investigate how *meso*-substituted C8Ph and Ph groups affect molecular packing and charge transport properties of BP derivatives. X-ray crystallography analysis confirms that all derivatives exhibit a herringbone packing structure. SC-OFETs using single crystals of each derivative demonstrate maximum hole mobilities of 1.64 cm<sup>2</sup> V<sup>-1</sup> s<sup>-1</sup> for C8Ph-BP, 0.89 cm<sup>2</sup> V<sup>-1</sup> s<sup>-1</sup> for C8Ph-Ph-BP, and 1.21 cm<sup>2</sup> V<sup>-1</sup> s<sup>-1</sup> for Ph-BP. The high mobility of C8Ph-BP is attributed to its interdigitated parallel  $\pi$ -stacking, enhanced by van der Waals interactions between *n*-octyl groups. In contrast, Ph-BP and C8Ph-Ph-BP show lower charge mobilities. This work demonstrates the influence of the *n*-octyl and *meso*-phenyl groups on the packing arrangements and the charge transport efficiency in SC-OFETs, offering insights into optimizing organic semiconductors for high-performance electronic applications.

sensors, and low-cost electronics.<sup>[4]</sup> A key challenge in this field is to enhance the charge-carrier mobility, which largely depends on the molecular packing and interactions within the solid-state structures of these materials.

Among small-molecule organic semiconductors, rod-like molecules such as acenes and thienoacenes have been extensively studied due to their relatively high charge mobility and predictable packing behavior.<sup>[5–8]</sup> In these materials, the substitution of functional groups plays a pivotal role in modulating the  $\pi$ - $\pi$  stacking interactions and packing structures, which are crucial for improving device performance. For instance, Anthony and coworkers demonstrated that substituents such as trimethylsilyl(TMS)-ethynyl, triisopropylsilyl(TIPS)-ethynyl, and other bulky groups could effectively tailor

## 1. Introduction

Organic semiconductors have garnered significant attention in recent years due to their potential for lightweight, flexible, and solution-processable electronic devices, such as organic field-effect transistors (OFETs).<sup>[1–3]</sup> Their unique characteristics make them promising candidates for applications in flexible displays,

the packing of pentacene molecules, resulting in enhanced charge transport properties (Figure 1A).<sup>[9–11]</sup> Another example, symmetrical [1]benzothieno[3,2-*b*][1]benzothiophene (BTBT), has two substituents at the end of the rod-shaped structure (Figure 1B).<sup>[2,12–15]</sup> The two linear alkyl groups showed clear dependency of charge carrier mobility on alkyl chain lengths because of the van der Waals interaction between alkyl groups. Asymmetric 2-decyl-7-phenyl[1]benzothieno[3,2-*b*][1]benzothiophene (Ph-BTBT-10) was liquid crystalline-type materials with FET hole mobility ( $\mu_h$ ) over 10 cm<sup>2</sup> V<sup>-1</sup> s<sup>-1</sup> (Figure 1C).<sup>[15]</sup>

Tetrabenzoporphyrins (BPs) are another class of promising p-type organic semiconductors with a unique square-shaped structure that exhibits strong  $\pi$ - $\pi$  interactions.<sup>[24–27]</sup> These interactions lead to stable solid-state structures but also limit the flexibility of molecular rotation compared to rod-like molecules. While unsubstituted BPs generally form cofacial herringbone packing in single crystals,<sup>[28]</sup> they are insoluble in common organic solvents, limiting their processability. Therefore, the introduction of substituents is necessary to render these materials soluble and suitable for solution processing techniques like dip coating and spin coating.

K. Miyazaki, K. Teranishi, H. Matsuda, K. Matsuo, M. Yamauchi, Y. Mizuhata, N. Shioya, T. Hasegawa, H. Yamada  
Institute for Chemical Research  
Kyoto University  
Gokasho, Uji, Kyoto 611-0011, Japan  
E-mail: [hyamada@scl.kyoto-u.ac.jp](mailto:hyamada@scl.kyoto-u.ac.jp)

The ORCID identification number(s) for the author(s) of this article can be found under <https://doi.org/10.1002/admi.202400946>

© 2025 The Author(s). Advanced Materials Interfaces published by Wiley-VCH GmbH. This is an open access article under the terms of the Creative Commons Attribution License, which permits use, distribution and reproduction in any medium, provided the original work is properly cited.

DOI: 10.1002/admi.202400946

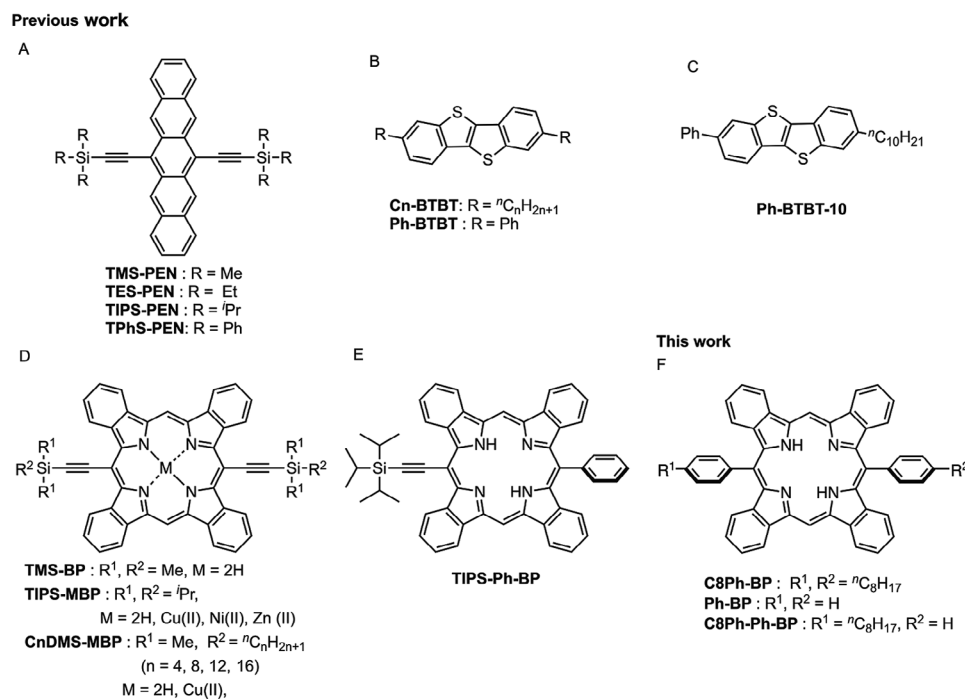


**Figure 1.** Molecular structures discussed in this paper: A) trialkylsilylethynyl-pentacene,<sup>[9–11]</sup> B) BTBT derivatives,<sup>[12–14]</sup> C) **Ph-BTBT-10**,<sup>[15]</sup> D) symmetrical 5,15-disubstituted BPs,<sup>[16–22]</sup> E) asymmetrical 5,15-disubstituted BP,<sup>[23]</sup> F) symmetrical and asymmetrical 5,15-bisaryl-BPs.

Previous research has demonstrated that 5,15-di(TMS-ethynyl)-BP (**TMS-BP**) led to herringbone structures but insufficient solubility for practical processing.<sup>[16–18]</sup> By changing one of the methyl groups of TMS-group in **TMS-BP** to an *n*-octyl (C8) or *n*-dodecyl (C12) group, the copper porphyrins, **C8DMS-CuBP** and **C12DMS-CuBP**, achieved OFET mobility of 4.1 cm<sup>2</sup> V<sup>-1</sup> s<sup>-1</sup> with stability up to 200 °C.<sup>[24]</sup> Additionally, BPs substituted with TIPS-ethynyl groups (**TIPS-BP**) exhibited polymorphism, yielding both brickwork and 1D packing structures depending on crystallization conditions.<sup>[20]</sup> The single crystal (SC)-OFET of **TIPS-BP** showed comparable performance with **TIPS-PEN** with an average hole mobility ( $\mu_{h,ave}$ ) of 2.4 cm<sup>2</sup> V<sup>-1</sup> s<sup>-1</sup> (the maximum hole mobility ( $\mu_{h,max}$ ): 6.1 cm<sup>2</sup> V<sup>-1</sup> s<sup>-1</sup>) and an average electron mobility ( $\mu_{e,ave}$ ) of 0.007 cm<sup>2</sup> V<sup>-1</sup> s<sup>-1</sup> (the maximum value electron mobility ( $\mu_{e,max}$ ): 0.029 cm<sup>2</sup> V<sup>-1</sup> s<sup>-1</sup>) by heating treatment of the crystalline film.<sup>[21,22]</sup>

In 2023, asymmetrically substituted 5-TIPS-ethynyl-15-phenyl-BP (**TIPS-Ph-BP**) was designed to encourage the face-to-face pairing of two molecules.<sup>[23]</sup> The single crystal structure, however, suggested the formation of a strongly interacting anti-parallel dimer followed by a 1D-arrangement of the dimer. As a result, **TIPS-Ph-BP** gave the slipped  $\pi$ -stacking structure with alternate two different porphyrin pairs A and B. The pairs A and B were alternating and the magnitude of the interaction of each pair was significantly different. The reason for the existence of the two different pairs came from the difference in size of TIPS-ethynyl and phenyl groups.

Inspired by the results above, we designed symmetric 5,15-bis(4-*n*-octylphenyl)BP (**C8Ph-BP**) and asymmetric 5-(4-*n*-octylphenyl)-15-phenyl-BP (**C8Ph-Ph-BP**) as the next generation. The phenyl groups at *meso*-position will improve the solubility

of the BPs and disturb the strong  $\pi$ - $\pi$  interaction resulting in the 1D-packing structure. With and without octyl groups at *para*-positions will influence the aligned arrangement of BPs by Van der Waals interaction between octyl groups. As the reference, 5,15-diphenyl-BP (**Ph-BP**) was also prepared. The packing structure of single crystals and SC-OFET performance were compared to clarify the effect of *meso*-phenyl groups and alkyl groups at *para*-positions of the phenyl groups.

## 2. Results and Discussion

### 2.1. Synthesis and Characterization

A series of BP derivatives were prepared following the previous report (**Figure 2**). An asymmetric precursor, **C8Ph-Ph-CP**, was synthesized by [2 + 2] acid-catalyzed condensation reaction of dipyrromethene **1**<sup>[16]</sup> using two kinds of aldehydes, 4-*n*-octylbenzaldehyde (**2**)<sup>[29]</sup> and benzaldehyde (**3**), in the presence of boron trifluoride etherate (BF<sub>3</sub>•OEt<sub>2</sub>), followed by oxidation with 2,3-dichloro-5,6-dicyano-1,4-benzoquinone (DDQ). Asymmetric **C8Ph-Ph-CP** was isolated by silica gel column chromatography and reprecipitation in 14% yield, with **C8Ph-CP** and **Ph-CP** as by-products in 8.5 and 14%, respectively. Symmetric **C8Ph-CP** and **Ph-CP** were prepared separately by [2 + 2] acid-catalyzed condensation reactions of dipyrromethene **1** and aldehyde **2** or **3**, respectively, in 21 and 57%, respectively. **C8Ph-Ph-CP**, **C8Ph-CP**, and **PhCP** were heated at 200 °C in a glass tube oven under vacuum to afford **C8Ph-BP**, **C8Ph-Ph-BP**, and **Ph-BP**, quantitatively. The obtained derivatives were characterized by <sup>1</sup>H-NMR, <sup>13</sup>C-NMR, and high-resolution mass spectroscopy (Figures S14–S31, Supporting Information).

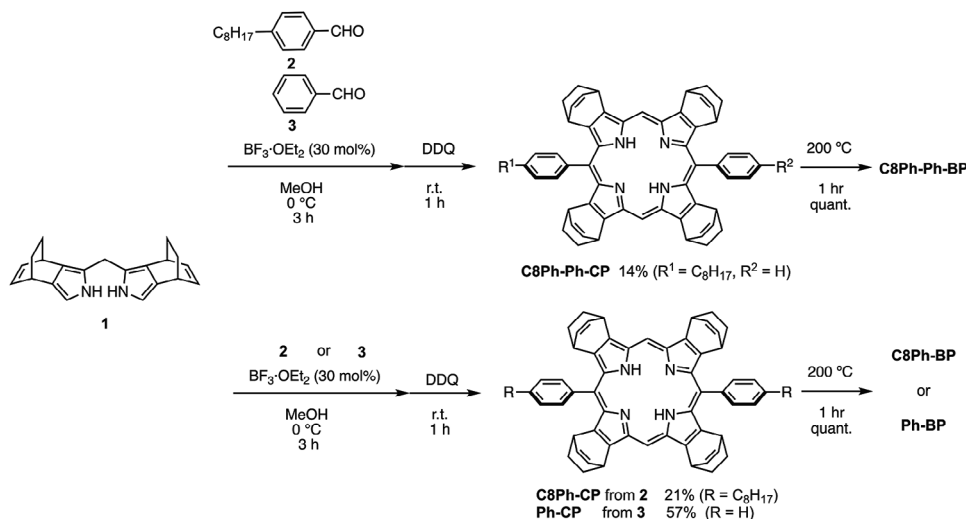


Figure 2. Synthesis scheme of C8Ph-Ph-BP, C8Ph-BP, and Ph-BP.

The UV-vis absorption spectra of BPs were measured in CHCl<sub>3</sub> (Figure 3). The Soret bands in absorption spectra were observed at 425 and 438 nm, and Q bands were at 572, 612, and 667 nm for the three BPs. The cyclic voltammetry (CV) and differential pulse voltammetry (DPV) of C8Ph-Ph-BP, C8Ph-BP, and Ph-BP were also measured to reveal the substitution effect on the electrochemical property (Figure 4; Figure S1, Supporting Information). These porphyrins showed two reversible oxidation waves ( $E_{ox}$ ) and one reduction waves ( $E_{red}$ ):  $E_{ox} = 0.08$  and  $0.25$  V (vs Fc/Fc<sup>+</sup>) and  $E_{red} = -1.69$  V (vs Fc/Fc<sup>+</sup>) for C8Ph-BP,  $E_{ox} = 0.09$  and  $0.27$  V (vs Fc/Fc<sup>+</sup>) and  $E_{red} = -1.69$  V (vs Fc/Fc<sup>+</sup>) for C8Ph-Ph-BP, and  $E_{ox} = 0.12$  and  $0.27$  V (vs Fc/Fc<sup>+</sup>) and  $E_{red} = -1.67$  V (vs Fc/Fc<sup>+</sup>) for Ph-BP.

## 2.2. Molecular Packing in Single Crystals

X-ray diffraction (XRD) analyses of single crystals were performed for C8Ph-BP, C8Ph-Ph-BP, and Ph-BP. Single crystals of C8Ph-BP and C8Ph-Ph-BP were obtained from toluene and *n*-octane, and those of Ph-BP were from THF and *n*-octane us-

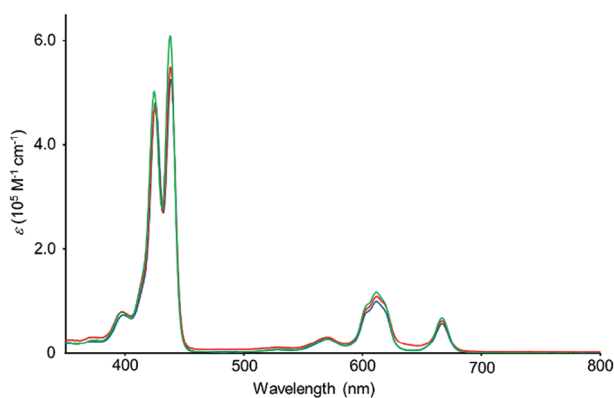


Figure 3. UV-vis absorption spectra of C8Ph-BP (blue), C8Ph-Ph-BP (red), and Ph-BP (green) in CHCl<sub>3</sub>.

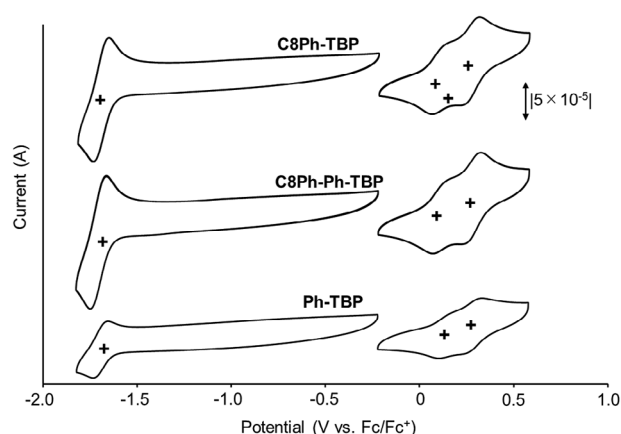


Figure 4. Cyclic voltammogram of C8Ph-BP (upper), C8Ph-Ph-BP (middle), and Ph-BP (lower). Solvent: CH<sub>2</sub>Cl<sub>2</sub>, electrolyte: 0.1 M *n*-Bu<sub>4</sub>NPF<sub>6</sub>, working electrode: glassy carbon; counter electrode: Pt wire, reference electrode: Ag/AgNO<sub>3</sub> (0.1 M in CH<sub>3</sub>CN) electrode; scan rate: 0.1 V s<sup>-1</sup>.

ing a vapor diffusion method (Figure S2, Supporting Information). The corresponding crystallographic parameters and data are summarized in Table S1 (Supporting Information), and ellipsoid plots of molecules are provided in Figures 5 and S3 (Supporting Information). Phenyl groups at *meso*-positions are highly tilted from the porphyrin planes: 85.07° for C8Ph-BP, 87.45° and 89.13° for phenyl groups and octyl phenyl groups of C8Ph-Ph-BP, and 87.53° for Ph-BP (Figure S3, Supporting Information). All of them showed herringbone packing structures with  $\pi$ - $\pi$  distances between porphyrin planes of 3.460, 3.477, and 3.489 Å for C8Ph-BP, C8Ph-Ph-BP, and Ph-BP, respectively. They showed slipped-stack packing arrangement, with perpendicular phenyl groups at *meso*-positions.

The octyl groups at the *para*-position are in all-antiperiplanar conformation, extending the length of the molecular long axis of 37.5 Å for C8Ph-BP. The octyl groups interdigitated with the neighboring molecules, creating a layered structure. This differs from layer-by-layer structures of C<sub>12</sub>-BTBT consisting of al-

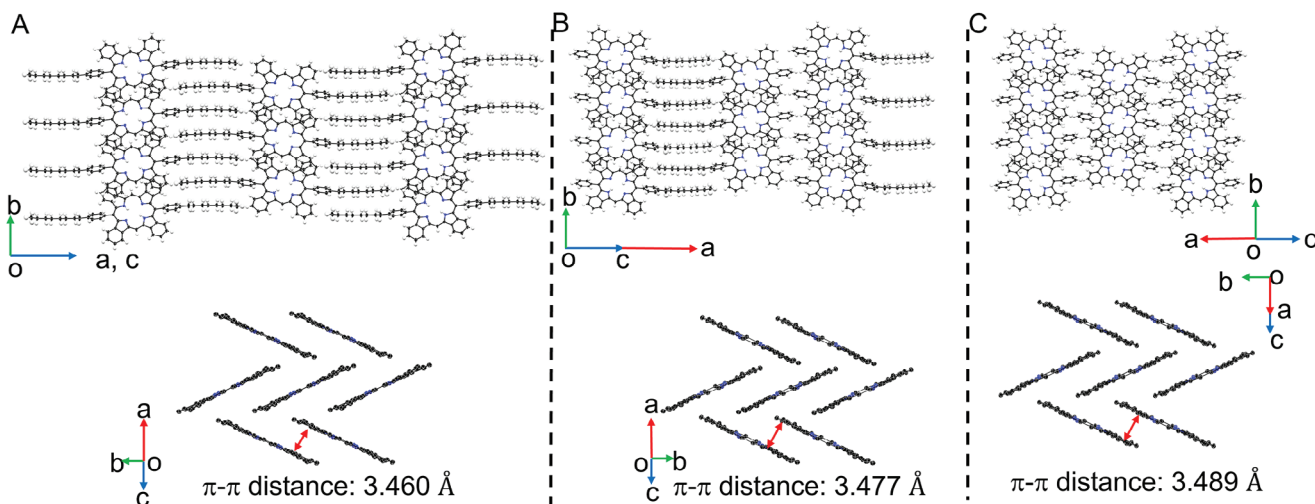


Figure 5. Packing structure in single crystals of A) C8Ph-BP, B) C8Ph-Ph-BP, and C) Ph-BP.

ternatively stacked aliphatic layers and BTBT core layers.<sup>[14]</sup> The alkyl groups of C<sub>12</sub>-BTBT don't interpenetrate each other as in C8Ph-BP. This difference likely arises from the contrasting aromatic frameworks, with C12-BTBT being rod-like and C8Ph-BP being square-like. C8Ph-Ph-BP exhibited an interdigitated bilayer-type parallel slipped  $\pi$ -stacking. Due to the van der Waals interactions of the octyl groups, anti-parallel packing like TIPS-Ph-BP<sup>[22]</sup> was not obtained for C8Ph-Ph-BP. Ph-BP also demonstrated a layered structure by CH- $\pi$  interaction.

To discuss charge transport properties in single crystals in detail, the charge transfer integrals ( $t$ ) of the highest occupied molecular orbitals (HOMOs) between the neighboring molecular pairs were calculated using the ADF2023 program<sup>[30]</sup> at the PBE/TZ2P level of theory (Figure S4 and Table S2, Supporting Information). Along the  $\pi$ -stacking direction (the crystallographic  $b$ -axis), the  $t$  values were 38.3, 28.6, and 22.3 meV, for C8Ph-BP, C8Ph-Ph-BP, and Ph-BP, respectively. The  $t$  value of pair A for C8Ph-BP is 1.5 times larger than that of Ph-BP. C8Ph-Ph-BP showed the middle value of C8Ph-BP and Ph-BP. TIPS-Ph-BP showed nonequivalent alternative values of 62.3 and 15.9 meV in  $b$ -axis direction, but C8Ph-Ph-BP showed one  $t$  value in the  $b$ -axis direction, which suggests the balanced packing of asymmetrical C8Ph-Ph-BP. The  $t$  values along the crystallographic  $c$ -axis (pairs B and C) were moderate and in the range of 7.1–7.9 meV for C8Ph-BP, C8Ph-Ph-BP, and Ph-BP. This is because the phenyl groups are common for all of the three BPs and the packing structures of porphyrin frameworks are similar to each other.

### 2.3. Hole Mobility in Single Crystals

The hole transport capability in SC-OFETs of BP derivatives was evaluated with the bottom-gate-top-contact (BGTC) structure (see Experimental Section and Supporting Information for the details of device fabrication and measurements). The optical and crossed-Nicols polarized micrographs of the best-performing devices of C8Ph-BP, C8Ph-Ph-BP, and Ph-BP are shown in Figure 6.

The obtained FET parameters are summarized in Table 1,

while the transfer curves of the best-performing devices are shown in Figure 7 and Figures S8–S10 (Supporting Information) with the corresponding output curves. The  $\mu_{h,max}$  ( $\mu_{h,ave}$ ) of C8Ph-BP, C8Ph-Ph-BP, and Ph-BP were 1.64 (1.18), 0.89 (0.51) and 1.21 (0.73) cm<sup>2</sup> V<sup>-1</sup> s<sup>-1</sup>, respectively. Symmetric C8Ph-BP showed the best performance and the asymmetric C8Ph-Ph-BP was about half of C8Ph-BP, but the number of octyl groups at *para*-position of phenyl groups did not dras-

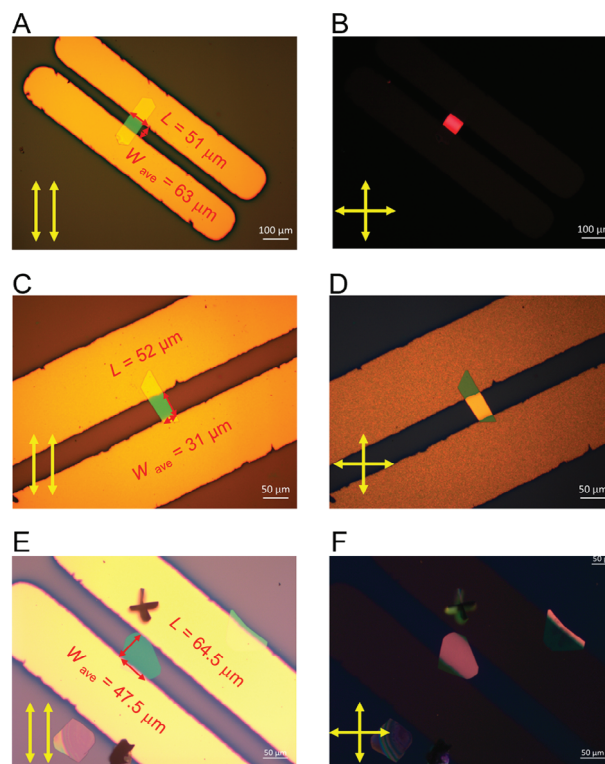


Figure 6. A,C,E) Optical and B,D,F) crossed-Nicols polarized micrographs of the best performing OFET (Device 1) of (A,B) C8Ph-BP, (C,D) C8Ph-Ph-BP, and (E,F) Ph-BP.

**Table 1.** SC-OEFT Characteristics of **C8Ph-BP**, **C8Ph-Ph-BP**, and **Ph-BP**.

Compounds	$\mu_{h,max}^a)$ [cm <sup>2</sup> V <sup>-1</sup> s <sup>-1</sup> ]	$\mu_{h,ave}^b)$ [cm <sup>2</sup> V <sup>-1</sup> s <sup>-1</sup> ]	$V_{th}^c)$ [V]	$I_{on}/I_{off}^c)$
<b>C8Ph-BP</b>	1.64	1.18 ± 0.32	-8	1.5 × 10 <sup>3</sup>
<b>C8Ph-Ph-BP</b>	0.89	0.51 ± 0.28	-13	7.6 × 10 <sup>2</sup>
<b>Ph-BP</b>	1.21	0.73 ± 0.28	-6	7.1 × 10 <sup>2</sup>

<sup>a)</sup> Hole mobility of the champion devices; <sup>b)</sup> Hole mobility of the average of 7, 6, and 11 devices for **C8Ph-BP**, **C8Ph-Ph-BP**, and **Ph-BP**, respectively; <sup>c)</sup> Data of the champion devices.

tically affect the charge carrier mobilities. This is probably because of the similar herringbone structure of these three compounds (Figure 5). The mobility stability was checked for **C8Ph-BP** and **C8Ph-Ph-BP**. It should be noted that nearly identical curves were observed after 10 cycles for **C8Ph-BP** and **C8Ph-Ph-BP**, (Figure S11, Supporting Information), suggesting the good bias-stress stability of SC-FETs

Out-of-plane XRD profiles of single crystals prepared for SC-OFET were measured (Figure 8; Figure S12, Supporting Information). **C8Ph-BP** and **C8Ph-Ph-BP** showed clear peaks of (h00) with  $d$  spacing ( $d$ ) = 18.8 and 31.9 Å, respectively. The peaks agreed well with the simulated (h00) peaks from single crystal data with 19.0 and 31.9 Å for **C8Ph-BP** and **C8Ph-Ph-BP**, respectively. Face index analysis of **C8Ph-BP** and **C8Ph-Ph-BP** based on the sin-

gle crystal XRD analyses revealed that the crystal face with the largest area of the platelet crystal corresponds to the (100) face. These results suggest that the crystallographic  $bc$  plane, which contains  $\pi$ -stacking direction, is parallel to the substrate and current flow direction (Figure S13, Supporting Information). For **Ph-BP**, experimental peaks were weak and three 100 peak series at  $d = 14.8, 12.8,$  and  $9.8$  Å were observed. The simulated (h00) peaks from single crystal data (Figure 5c) suggested  $d = 12.8$  Å, which is a minor structure. The other two peaks are assignable to different packing structures because they did not agree with the other simulated peaks from the single crystal data (Figure S13, Supporting Information). These results indicated the presence of crystal polymorphism, which was observed by optical microscopy.

Here, we consider why the average hole mobility of **C8Ph-BP** is two times higher than that of **C8Ph-Ph-BP**. One reasonable reason is that **C8Ph-BP** has a more appropriate packing structure enabling superior charge transport as revealed by theoretical estimation. In addition, the interdigitation between octyl groups can contribute to the stabilization of packing structures between the BP core units via intermolecular van der Waals interactions. Considering this stabilization effect, the **C8Ph-Ph-BP** should act efficiently compared to the case of **C8Ph-BP**, where the BP core of **C8Ph-Ph-BP** is fixed at both sides, leading to the successive interlayer connection without interruption. This suppresses a thermal vibration of BP cores that gives rise to a decrease in charge mobility.

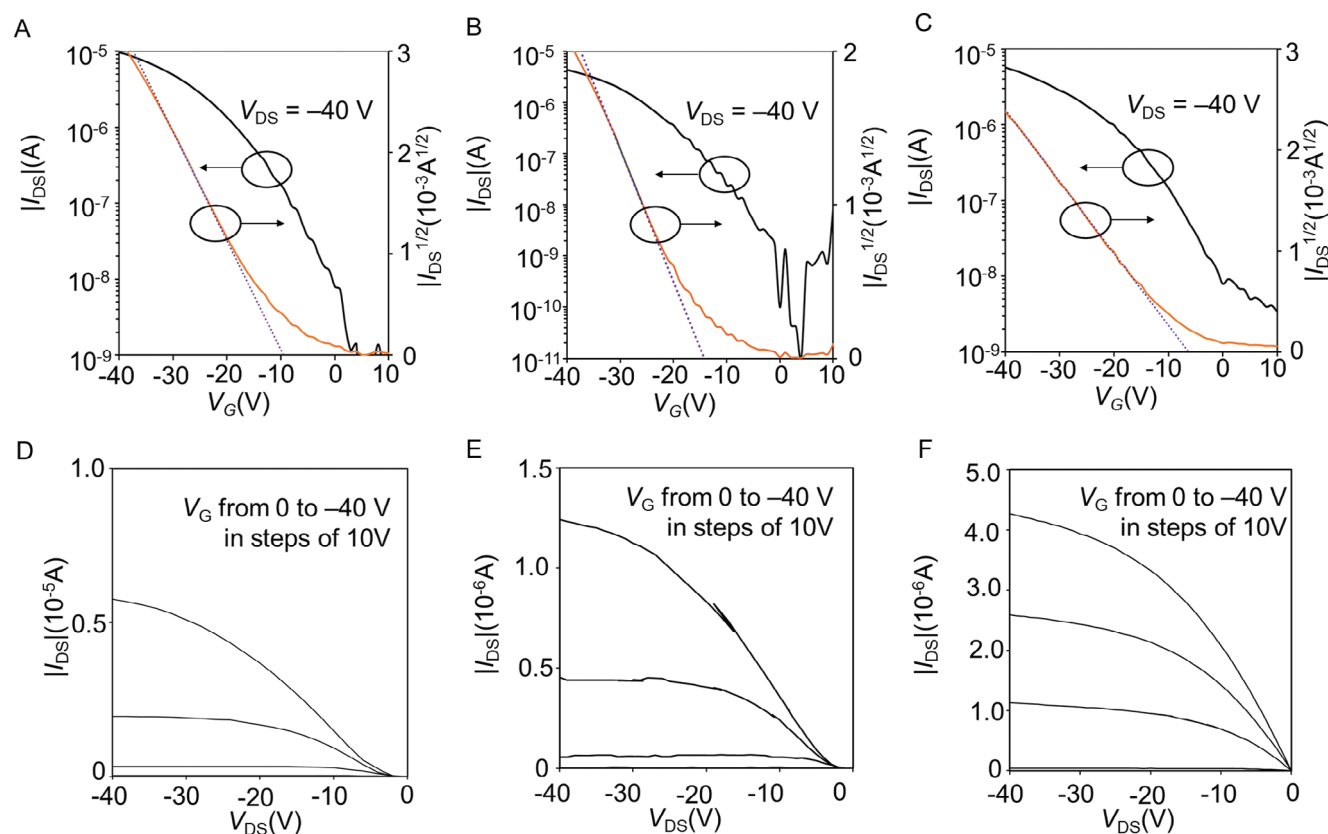


**Figure 7.** The best transfer characteristics A–C) and output characteristics D–F) of BGTC SC-OFETs of (A, D) **C8Ph-BP**, (B, E) **C8Ph-Ph-BP**, and (C, F) **Ph-BP**.

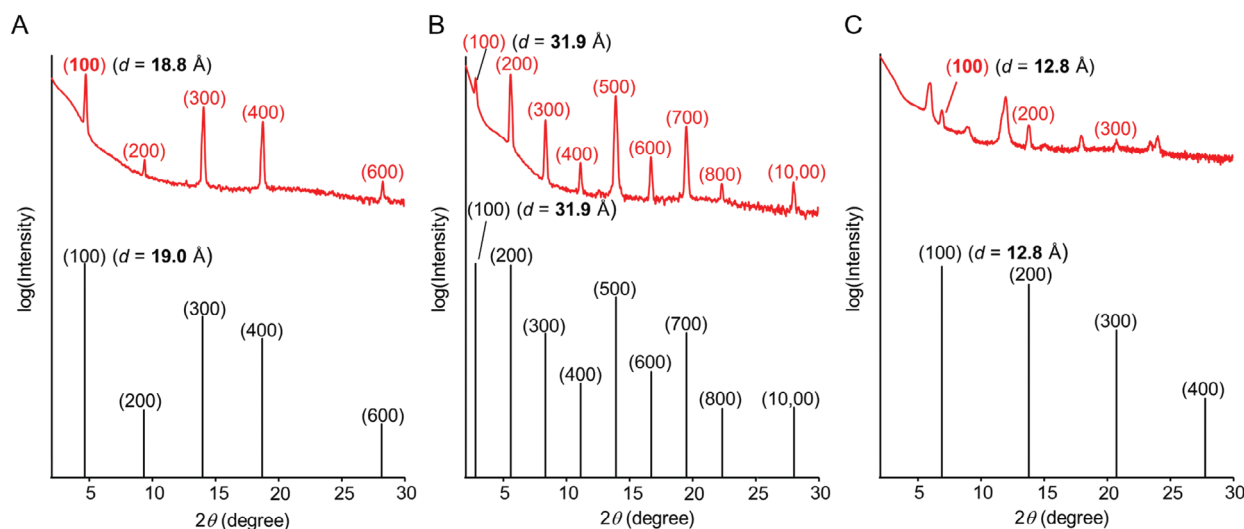


**Figure 8.** Out-of-plane XRD profiles of single crystals for SC-OFET (upper) and simulated (h00) peaks from single crystal XRD analysis data of Figure 5 (lower). A) **C8Ph-BP**, B) **C8Ph-Ph-BP**, and C) **Ph-BP**.

For the scalability of the devices, solution sharing of the film is important, but unfortunately, the dip-coated film of **C8Ph-BP** could not survive during the vacuum deposition of the gold electrodes. Considering **C8DMS-CuBP** and **C12DMS-CuBP** gave stable films by dip-coating until 200 °C,<sup>[19]</sup> phenyl groups perpendicular to the porphyrin framework might reduce the stability of the BP packing structure.

### 3. Conclusion

In this study, we synthesized and characterized three 5,15-bisaryl-tetrabenzoporphyrin derivatives: **C8Ph-BP**, **C8Ph-Ph-BP**, and **Ph-BP**, to investigate how *meso*-substituted phenyl and *n*-octyl groups affect molecular packing and charge transport properties in single crystals. Single-crystal XRD analyses revealed that all derivatives exhibit herringbone packing structures, with notable  $\pi$ - $\pi$  interactions between porphyrin planes. The octyl groups in **C8Ph-BP** and **C8Ph-Ph-BP** formed parallel slipped  $\pi$ -stacking with interdigitated layer-by-layer structure, while **Ph-BP** exhibited a layered structure without interdigitation. Among the derivatives, **C8Ph-BP** demonstrated the highest performance in SC-OFETs, followed by **Ph-BP** and **C8Ph-Ph-BP**. The results show that the presence of two *n*-octyl groups plays a significant role in enhancing the packing structure and, consequently, the charge carrier mobility. One *n*-octyl group in a molecule is not so effective and the charge carrier mobility of **C8Ph-Ph-BP** is less than that of **Ph-BP**. The findings emphasize the importance of fine-tuning molecular substituents to optimize packing and improve the charge transport properties of organic semiconductors, offering valuable insights for the design of high-performance OFET materials.

### 4. Experimental Section

**General:** All reagents and solvents were purchased from FUJIFILM Wako, Kanoto Chemical, Nacalai Tesque, Tokyo Chemical Industry (TCI), or Sigma-Aldrich, and were used as received. Thin layer chromatography

(TLC) was performed on the Merck KGaA 105554 silica gel plates. <sup>1</sup>H and <sup>13</sup>C NMR spectra were recorded using JEOL ECS-400, Bruker Avance NEO 400, or Bruker Avance III 600 spectrometer at ambient temperature. Chemical shifts of <sup>1</sup>H and <sup>13</sup>C signals were quoted to tetramethylsilane (*d* = 0.00 ppm) as an internal standard or with reference to residual solvent signals of CHCl<sub>3</sub> (7.26 ppm for <sup>1</sup>H and 77.16 ppm for <sup>13</sup>C). High-resolution mass spectra (HR-MS) were collected by a Bruker solarix FT-ICR (MALDI) or Bruker timsTOF (APCI-MS) instrument. UV-vis absorption spectra were measured using a JASCO UV-Visible/NIR spectrophotometer V-670. Cyclic voltammetry was performed on an ALS 612D electrochemical analyzer and a three-electrode cell equipped with a glassy carbon electrode, a Pt wire, and an Ag/AgNO<sub>3</sub> (0.1 m in CH<sub>3</sub>CN) electrode as a working, a counter, and a reference electrode, respectively. XRD data were collected on a Bruker D8 VENTURE system (PHOTON III 14 with I $\mu$ S Diamond), using Mo K $\alpha$  radiation ( $\lambda$  = 0.71073 Å). Out-of-plane XRD measurements of the single crystals for FET were performed using a Rigaku SmartLab X-ray diffractometer with a Cu-K $\alpha$  source ( $\lambda$  = 1.5418 Å) in the  $\theta$ - $2\theta$  scan mode at scattering angles of 2–30°.

**Synthesis:** Bicyclo[2.2.2]octadiene-fused dipyrromethene **1** was prepared according to the literature.<sup>[16]</sup>

**4-*n*-Octylbenzaldehyde:** A solution of *n*-butyllithium in hexane (1.56 m, 13.1 mL, 20.5 mmol) was added dropwise to a solution of 1-bromo-4-octylbenzene (5.00 g, 18.6 mmol) in THF (30 mL) at -78 °C under Ar. The resulting mixture was stirred at -78 °C. After 30 min, *N,N*-dimethylformamide (2.71 mL, 37.2 mmol) was added to the reaction. The mixture was warmed to room temperature and poured into a separatory funnel with H<sub>2</sub>O and ethyl acetate and partitioned. The organic phase was collected, and the aqueous phase was extracted with ethyl acetate twice. The combined organic extract was washed with brine, dried over Na<sub>2</sub>SO<sub>4</sub>, and concentrated under reduced pressure. The residue was purified by column chromatography on silica gel (dichloromethane) to provide 4-*n*-octylbenzaldehyde as a colorless liquid in 87% yield (3.52 g, 16.1 mmol). <sup>1</sup>H NMR (400 MHz, CDCl<sub>3</sub>,  $\delta$ ): 9.97 (s, 1 H; CHO), 7.79 (d, *J* = 8.2 Hz, 2H; Ar H), 7.33 (d, *J* = 8.0 Hz, 2H; Ar H), 2.68 (t, *J* = 7.6 Hz, 2H; CH<sub>2</sub>), 1.64 (tt, *J* = 7.5 Hz, 2H; CH<sub>2</sub>), 1.37–1.21 (m, 12 H; CH<sub>2</sub>), 0.88 ppm (t, *J* = 6.7 Hz, 3H; CH<sub>3</sub>); <sup>13</sup>C NMR (101 MHz, CDCl<sub>3</sub>,  $\delta$ ): 192.25, 150.69, 134.49, 130.05, 129.23, 36.37, 32.00, 31.24, 29.55, 29.41, 29.63, 22.80, 14.25 ppm; HRMS (APCI-MS): *m/z* [M + H]<sup>+</sup> Calcd for C<sub>15</sub>H<sub>23</sub>O: 219.1743; found: 219.1745.

**Bicyclo[2.2.2]octadiene-fused 5,15-bis(4-*n*-octylphenyl)porphyrin (C<sub>8</sub>Ph-CP):** A solution of compound **1** (687.4 mg, 2.3 mmol) in MeOH (245 mL) was deoxygenated by bubbling argon gas for 20 min. After addition of 4-*n*-octylbenzaldehyde (543.6 mg, 2.5 mmol), BF<sub>3</sub>·OEt<sub>2</sub>, (0.087 mL,

0.69 mmol) was added dropwise to the mixture at 0 °C. The resulting mixture was stirred for 3 h at 0 °C. DDQ (1.0 g, 4.3 mmol) was added to the mixture, and the solution was stirred for 1 h at room temperature. Then, the solvent was removed under reduced pressure. The residue was purified by alumina column chromatography (CHCl<sub>3</sub>) and silica gel column chromatography (CHCl<sub>3</sub>) to give **C8Ph-CP** as a red solid in 21% yield (242.1 mg, 0.242 mmol). Note that these products were isolated as a mixture of stereoisomers regarding the orientation of the bicyclo[2.2.2]octadieno units. <sup>1</sup>H NMR (600 MHz, CDCl<sub>3</sub>, δ): 10.34 (s, 2H), 8.22 – 8.06 (m, 4H; Ar H), 7.66 – 7.58 (m, 4H; Ar H), 7.04 – 6.98 (m, 4H; Ar H), 6.74 – 6.68 (m, 4H; Ar H), 5.70 (s, 4H; CH), 3.80 (s, 4H; CH), 3.09 (t, J = 7 Hz, 4H; CH<sub>2</sub>), 2.07 – 2.05 (m, 4H; CH<sub>2</sub>), 2.02 – 1.97 (m, 4H; CH<sub>2</sub>), 1.91 – 1.78 (m, 4H; CH<sub>2</sub>), 1.72 – 1.70 (m, 4H; CH<sub>2</sub>), 1.67 – 1.52 (m, 10H; CH<sub>2</sub>), 1.51 – 1.43 (m, 6H; CH<sub>2</sub>), 1.42 – 1.38 (m, 8H; CH<sub>2</sub>), 0.96 (t, J = 7 Hz, 6H; CH<sub>3</sub>), -3.83 (s, 2H; NH); <sup>13</sup>C NMR (151 MHz, CDCl<sub>3</sub>, δ): 150.6, 150.6, 150.5, 148.6, 142.9, 140.3, 139.8, 137.4, 137.2, 137.2, 136.3, 136.2, 133.2, 133.1, 132.9, 126.8, 126.7, 126.6, 116.9, 116.9, 116.8, 97.0, 96.9, 37.8, 37.8, 36.1, 36.0, 32.0, 31.8, 29.7, 29.6, 29.1, 27.7, 27.2, 22.8, 14.2; HRMS (MALDI) *m/z*: [M]<sup>+</sup> calcd for C<sub>72</sub>H<sub>78</sub>N<sub>4</sub>, 998.62210; found, 998.62246.

**Bicyclo[2.2.2]octadiene-fused 5-phenyl-15-(4-n-octylphenyl)porphyrin (C8Ph-Ph-CP)**: A solution of compound **1** (394.4 mg, 1.3 mmol) in MeOH (140 mL) was deoxygenated by bubbling of argon gas for 20 min. After addition of 4-*n*-octylbenzaldehyde (170.3 mg, 0.78 mmol) and benzaldehyde (84.5 mg, 0.78 mmol), BF<sub>3</sub>·OEt<sub>2</sub> (0.050 mL, 0.39 mmol) was added dropwise to the mixture at 0 °C. The resulting mixture was stirred for 3 h at 0 °C. DDQ (598 mg, 2.6 mmol) was added to the mixture, and the solution was stirred for 1 h at room temperature. Then, the solvent was removed under reduced pressure. The residue was purified by alumina column chromatography (CHCl<sub>3</sub>), silica gel column chromatography (CHCl<sub>3</sub>) and GPC (CHCl<sub>3</sub>) to give **C8Ph-Ph-CP** as a red solid in 14% yield (78.3 mg, 0.088 mmol), **C8<sub>8</sub>Ph-CP** as a red solid in 8.5% yield (55.2 mg, 0.055 mmol) and **Ph-CP** as a red solid in 14% yield (70.4 mg, 0.091 mmol). Note that these products were isolated as a mixture of stereoisomers regarding the orientation of the bicyclo[2.2.2]octadieno units. **C8Ph-Ph-CP**: <sup>1</sup>H NMR (600 MHz, CDCl<sub>3</sub>, δ): 10.36 (s, 2H), 8.33 – 8.06 (m, 4H; Ar H), 7.93 (t, J = 8 Hz, 1H; Ar H), 7.87 – 7.78 (m, 2H; Ar H), 7.66 – 7.58 (m, 2H; Ar H), 7.04 – 6.98 (m, 4H; Ar H), 6.72 – 6.70 (m, 4H; Ar H), 5.70 (s, 4H; CH), 3.80 (s, 2H; CH), 3.75 (s, 2H; Ar H), 3.09 (t, J = 7 Hz, 2H; CH<sub>2</sub>), 2.08 – 2.05 (m, 4H; CH<sub>2</sub>), 2.02 – 1.97 (m, 2H; CH<sub>2</sub>), 1.91 – 1.78 (m, 4H; CH<sub>2</sub>), 1.74 – 1.70 (m, 4H; CH<sub>2</sub>), 1.65 – 1.58 (m, 8H; CH<sub>2</sub>), 1.47 – 1.42 (m, 2H; CH<sub>2</sub>), 1.40 – 1.38 (m, 4H; CH<sub>2</sub>), 0.96 (t, J = 7 Hz, 3H; CH<sub>3</sub>), -3.80 (s, 2H; NH); <sup>13</sup>C NMR (151 MHz, CDCl<sub>3</sub>, δ): 150.7, 150.7, 150.6, 148.6, 148.4, 142.9, 142.6, 140.4, 140.1, 139.8, 137.3, 137.2, 137.2, 137.2, 136.3, 136.2, 133.4, 133.2, 133.1, 133.0, 132.8, 128.3, 126.8, 126.7, 126.7, 126.6, 126.6, 126.5, 117.0, 117.0, 117.0, 116.0, 116.0, 116.0, 97.0, 97.0, 37.8, 37.8, 36.1, 36.0, 32.0, 31.8, 29.7, 29.6, 29.1, 27.6, 27.2, 22.8, 14.2; HRMS (MALDI) *m/z*: [M]<sup>+</sup> calcd for C<sub>64</sub>H<sub>62</sub>N<sub>4</sub>, 886.49690; found, 886.49635.

**Bicyclo[2.2.2]octadiene-fused 5,15-diphenylporphyrin (Ph-CP)**: A solution of compound **1** (50 mg, 0.16 mmol) in MeOH (20 mL) was deoxygenated by bubbling argon gas for 20 min. After the addition of benzaldehyde (0.02 mL, 0.2 mmol), BF<sub>3</sub>·OEt<sub>2</sub> (0.005 mL, 0.05 mmol) was added dropwise to the mixture at 0 °C. The resulting mixture was stirred for 3 h at 0 °C. DDQ (80 mg, 0.33 mmol) was added to the mixture, and the solution was stirred for 1 h at room temperature. Then, the solvent was removed under reduced pressure. The residue was purified by alumina column chromatography (CHCl<sub>3</sub>) and silica gel column chromatography (CHCl<sub>3</sub>) to give **Ph-CP** as a red solid in 57% yield (35.3 mg, 0.046 mmol). Note that these products were isolated as a mixture of stereoisomers regarding the orientation of the bicyclo[2.2.2]octadieno units. <sup>1</sup>H NMR (600 MHz, CDCl<sub>3</sub>, δ): 10.36 (s, 2H), 8.34 – 8.18 (m, 4H; Ar H), 7.93 (t, J = 8 Hz, 2H; Ar H), 7.87 – 7.78 (m, 4H; Ar H), 7.05 – 6.98 (m, 4H; Ar H), 6.74 – 6.68 (m, 4H; Ar H), 5.71 (s, 4H; CH), 3.75 (s, 4H; CH), 2.08 – 2.05 (m, 4H; CH<sub>2</sub>), 1.92 – 1.78 (m, 4H; CH<sub>2</sub>), 1.74 – 1.71 (m, 4H; CH<sub>2</sub>), 1.67 – 1.57 (m, 4H; CH<sub>2</sub>), -3.80 (s, 2H; NH); <sup>13</sup>C NMR (151 MHz, CDCl<sub>3</sub>, δ): 150.8, 150.7, 148.5, 142.6, 140.2, 137.3, 137.2, 137.2, 137.2, 136.3, 136.2, 133.4, 133.2, 133.0, 128.3, 126.7, 126.6, 126.5, 116.8, 116.7, 116.7, 97.1,

97.1, 37.8, 37.8, 36.1, 27.6, 27.6, 27.2; HRMS (MALDI) *m/z*: [M]<sup>+</sup> calcd for C<sub>56</sub>H<sub>46</sub>N<sub>4</sub>, 774.37170; found, 774.37204.

**5,15-Bis(4-*n*-octylphenyl)tetrabenzoporphyrin (C8Ph-BP)**: **C8Ph-CP** (12.1 mg, 12 μmol) was heated at 200 °C for 1 h under vacuum in a glass tube oven to give **C8 Ph-BP** as a green solid in 92% yield (9.8 mg, 11 μmol). **C8Ph-BP** was further purified by recrystallization with toluene and octane to provide a highly pure material for photophysical measurements and fabrications of OFETs. <sup>1</sup>H NMR (600 MHz, CDCl<sub>3</sub>, δ): 11.02 (s, 2H), 9.62 (d, J = 8 Hz, 4H; Ar H), 8.13 (d, J = 8 Hz, 4H; Ar H), 8.08 (t, J = 7 Hz, 4H; Ar H), 7.78 (d, J = 8 Hz, 4H; Ar H), 7.74 (t, J = 7 Hz, 4H; Ar H), 7.50 (d, J = 8 Hz, 4H; Ar H), 3.16 (t, J = 7 Hz, 4H; CH<sub>2</sub>), 2.09 – 2.04 (m, 4H; CH<sub>2</sub>), 1.72 – 1.67 (m, 4H; CH<sub>2</sub>), 1.62 – 1.58 (m, 4H; CH<sub>2</sub>), 1.54 – 1.49 (m, 4H; CH<sub>2</sub>), 1.46 – 1.43 (m, 8H; CH<sub>2</sub>), 1.00 (t, J = 7 Hz, 6H; CH<sub>3</sub>), -1.47 (s, 2H; NH); <sup>13</sup>C NMR (150 MHz, CDCl<sub>3</sub>, δ): 144.0, 141.8, 139.0, 138.8, 138.5, 137.0, 132.3, 129.2, 127.1, 126.7, 125.1, 120.9, 116.6, 92.9, 36.2, 32.1, 31.8, 29.8, 29.6, 29.3, 22.8, 14.2; HRMS (MALDI) *m/z*: [M]<sup>+</sup> calcd for C<sub>64</sub>H<sub>62</sub>N<sub>4</sub>, 886.49690; found, 886.49689. CCDC 2391322.

**5-Phenyl-15-(4-*n*-octylphenyl)tetrabenzoporphyrin (C8Ph-Ph-BP)**: **C8Ph-Ph-CP** (16.9 mg, 19 μmol) was heated at 200 °C for 1 h under vacuum in a glass tube oven to give **C8Ph-Ph-BP** as a green solid in 96% yield (14.1 mg, 18 μmol). **C8Ph-Ph-BP** was further purified by recrystallization with toluene and octane to provide a highly pure material for photophysical measurements and fabrications of OFETs. <sup>1</sup>H NMR (600 MHz, CDCl<sub>3</sub>, δ): 11.02 (s, 2H), 9.62 (d, J = 8 Hz, 4H; Ar H), 8.24 (d, J = 7 Hz, 2H; Ar H), 8.12 (d, J = 8 Hz, 2H; Ar H), 8.09 – 8.06 (m, 4H; Ar H), 7.97 (t, J = 8 Hz, 2H; Ar H), 7.78 (d, J = 8 Hz, 2H; Ar H), 7.74 (t, J = 7 Hz, 4H; Ar H), 7.50 (d, J = 8 Hz, 2H; Ar H), 7.43 (d, J = 8 Hz, 2H; Ar H), 3.16 (t, J = 7 Hz, 2H; CH<sub>2</sub>), 2.09 – 2.04 (m, 2H; CH<sub>2</sub>), 1.71 – 1.67 (m, 2H; CH<sub>2</sub>), 1.62 – 1.58 (m, 2H; CH<sub>2</sub>), 1.53 – 1.52 (m, 2H; CH<sub>2</sub>), 1.45 – 1.42 (m, 4H; CH<sub>2</sub>), 1.00 (t, J = 7 Hz, 3H; CH<sub>3</sub>), -1.46 (s, 1H; NH), -1.47 (s, 1H; NH); <sup>13</sup>C NMR (151 MHz, CDCl<sub>3</sub>, δ): 144.0, 141.3, 139.0, 138.4, 137.0, 136.9, 132.6, 129.2, 129.1, 127.2, 127.1, 126.8, 125.2, 125.0, 120.9, 120.9, 92.9, 36.2, 32.1, 31.8, 29.8, 29.6, 29.3, 22.8, 14.2; HRMS (MALDI) *m/z*: [M]<sup>+</sup> calcd for C<sub>56</sub>H<sub>46</sub>N<sub>4</sub>, 774.37170; found, 774.37128. CCDC 2391323.

**5,15-Diphenyltetrabenzoporphyrin (Ph-BP)**: **Ph-CP** (5.0 mg, 6.4 μmol) was heated at 200 °C for 1 h under vacuum in a glass tube oven to give **Ph-BP** as a green solid in 96% yield (4.1 mg, 6.2 μmol). **Ph-BP** was further purified by recrystallization with THF and octane to provide a highly pure material for photophysical measurements and fabrications of OFETs. <sup>1</sup>H NMR (600 MHz, CDCl<sub>3</sub>, δ): 11.09 (s, 2H), 9.66 (d, J = 8 Hz, 4H; Ar H), 8.28 (d, J = 7 Hz, 4H; Ar H), 8.09 (m, 6H; Ar H), 8.00 (t, J = 8 Hz, 4H; Ar H), 7.77 (t, J = 7 Hz, 4H; Ar H), 7.47 (d, J = 8 Hz, 4H; Ar H), -1.33 (s, 2H; NH); <sup>13</sup>C NMR (151 MHz, CDCl<sub>3</sub>, δ): 141.7, 141.3, 139.1, 138.9, 137.0, 132.6, 129.3, 129.1, 127.3, 126.9, 125.0, 121.0, 116.6, 93.0; HRMS (MALDI) *m/z*: [M]<sup>+</sup> calcd for C<sub>48</sub>H<sub>30</sub>N<sub>4</sub>, 662.24650; found, 662.24589; CCDC 2391321.

**Preparation Method of SC-OFET Devices**: Single crystals of **C8Ph-BP** for FET measurements were prepared as follows: 0.1 mL of xylene solution (0.25 g L<sup>-1</sup>) of **C8Ph-BP** was dropped on UV-O<sub>3</sub>-treated Si/SiO<sub>2</sub> substrate and kept in *n*-hexane vapor for 1 day at room temperature. Hexagonal plate-like single crystals were obtained (Figures S5 and S6, Supporting Information). Toluene and *n*-octane were used for rich and poor solvents for **C8Ph-Ph-BP** and THF/*o*-dichlorobenzene (1:1) and *n*-octane was used for **Ph-BP**. The single crystals of **C8Ph-Ph-BP** were hexagonal plate-like crystals (Figures S7 and S8, Supporting Information), but **Ph-BP** obtained on the substrate were a mixture of different shapes. Trapezoidal crystals, which were the major shapes among them, were used for SC-OFET fabrication (Figures S9 and S10, Supporting Information). **C8Ph-BP** and **C8Ph-Ph-BP** show plate-like and sharp structures while **Ph-BP** shows blunt shapes. On the obtained single crystals, gold source, and drain electrodes were vacuum deposited.

**Ethical Statement**: This study was conducted in accordance with the ethical principles set forth by the MEXT (Ministry of Education, Culture, Sports, Science and Technology), Japan.

## Supporting Information

Supporting Information is available from the Wiley Online Library or from the author.

## Acknowledgements

This work was supported by the Japan Society for the Promotion of Science (JSPS) KAKENHI Grant Numbers JP22K05255 to K.M., JP22K14556 to M.Y., JP24H01714 (Transformative Research Areas “Meso-Hierarchical Materials”) to M.Y., JP20H05833 (Transformative Research Areas “Dynamic Exciton”) to H.Y. This work was supported by the JST SPRING, Grant Number JPMJSP2110 to K.M. This study was supported by the Joint Usage/Research Center [JURC, Institute for Chemical Research (ICR), Kyoto University] by providing access to a Bruker Avance III 600 NMR spectrometer. The authors are furthermore grateful for the computation time, which was provided by the Super Computer Laboratory (ICR, Kyoto University).

## Conflict of Interest

The authors declare no conflict of interest.

## Author Contributions

The manuscript was written through the contributions of all authors. All authors have approved of the final version of the manuscript. K.M. did synthesis, characterization of compounds, DFT calculations, and OFET measurement. K.T. did synthesis and characterization of n-octylbenzaldehyde, K.M. supported the DFT calculations and OFET measurement, M.Y. supported the preparation of samples, Y.M. did the X-ray single crystal structure analysis. H.M., N.S. and T.H. conducted the out-of-plane XRD measurement and analyzed the results. H.Y. supervised the project and finalized the manuscript.

## Data Availability Statement

The data that support the findings of this study are available from the corresponding author upon reasonable request.

## Keywords

benzoporphyrins, single-crystal organic field-effect transistor, X-ray diffraction analysis, Single crystal structure

Received: November 25, 2024

Revised: January 21, 2025

Published online:

[1] J. E. Anthony, *Chem. Rev.* **2006**, *106*, 5028.

[2] K. Takimiya, S. Shinamura, I. Osaka, E. Miyazaki, *Adv. Mater.* **2011**, *23*, 4347.

- [3] K. Takimiya, M. Nakano, H. Sugino, I. Osaka, *Synth. Met.* **2016**, *217*, 68.
- [4] H. Sirringhaus, *Adv. Mater.* **2014**, *26*, 1319.
- [5] Y. Yamaguchi, Y. Kojiguchi, S. Kawata, T. Mori, K. Okamoto, M. Tsutsui, T. Koganezawa, H. Katagiri, T. Yasuda, *Chem. Mater.* **2020**, *32*, 5350.
- [6] T. Okamoto, C. P. Yu, C. Mitsui, M. Yamagishi, H. Ishii, J. Takeya, *J. Am. Chem. Soc.* **2020**, *142*, 9083.
- [7] M. L. Tang, T. Okamoto, Z. Bao, *J. Am. Chem. Soc.* **2006**, *128*, 16002.
- [8] C. Mitsui, T. Okamoto, M. Yamagishi, J. Tsurumi, K. Yoshimoto, K. Nakahara, J. Soeda, Y. Hirose, H. Sato, A. Yamano, T. Uemura, J. Takeya, *Adv. Mater.* **2014**, *26*, 4546.
- [9] J. E. Anthony, J. S. Brooks, D. L. Eaton, S. R. Parkin, *J. Am. Chem. Soc.* **2001**, *123*, 9482.
- [10] J. E. Anthony, D. L. Eaton, S. R. Parkin, *Org. Lett.* **2002**, *4*, 15.
- [11] C. D. Sheraw, T. N. Jackson, D. L. Eaton, J. E. Anthony, *Adv. Mater.* **2003**, *15*, 2009.
- [12] T. Izawa, E. Miyazaki, K. Takimiya, *Adv. Mater.* **2008**, *20*, 3388.
- [13] H. Ebata, T. Izawa, E. Miyazaki, K. Takimiya, M. Ikeda, H. Kuwabara, T. Yui, *J. Am. Chem. Soc.* **2007**, *129*, 15732.
- [14] K. Takimiya, H. Ebata, K. Sakamoto, T. Izawa, T. Otsubo, Y. Kunugi, *J. Am. Chem. Soc.* **2006**, *128*, 12604.
- [15] H. Iino, T. Usui, J. Hanna, *Nat. Commun.* **2015**, *6*, 6828.
- [16] H. Yamada, K. Kushibe, T. Okujima, H. Uno, N. Ono, *Chem. Commun.* **2006**, 383.
- [17] H. Yamada, K. Kushibe, S. Mitsuogi, T. Okujima, H. Uno, N. Ono, *Tetrahedron Lett.* **2008**, *49*, 4731.
- [18] K. Takahashi, N. Yamada, D. Kumagai, D. Kuzuhara, M. Suzuki, Y. Yamaguchi, N. Aratani, K. Nakayama, H. Yamada, *J. Porphyrins Phthalocyanines* **2015**, *19*, 465.
- [19] E. Jeong, T. Ito, K. Takahashi, T. Koganezawa, H. Hayashi, N. Aratani, M. Suzuki, H. Yamada, *ACS Appl. Mater. Interfaces* **2022**, *14*, 32319.
- [20] K. Takahashi, B. Shan, X. Xu, S. Yang, T. Koganezawa, D. Kuzuhara, N. Aratani, M. Suzuki, Q. Miao, H. Yamada, *ACS Appl. Mater. Interfaces* **2017**, *9*, 8211.
- [21] J. Zhu, H. Hayashi, M. Chen, C. Xiao, K. Matsuo, N. Aratani, L. Zhang, H. Yamada, *J. Mater. Chem. C* **2022**, *10*, 2527.
- [22] G. Xue, B. Peng, T. Ye, J. Wu, Y. Zhao, Y. Liu, H. Yamada, H. Chen, H. Li, *Adv. Electron. Mater.* **2022**, *8*, 202200158.
- [23] K. Miyazaki, K. Matsuo, H. Hayashi, M. Yamauchi, N. Aratani, H. Yamada, *Org. Lett.* **2023**, *25*, 7354.
- [24] S. Aramaki, Y. Sakai, N. Ono, *Appl. Phys. Lett.* **2004**, *84*, 2085.
- [25] P. B. Shea, J. Kanicki, L. R. Pattison, P. Petroff, M. Kawano, H. Yamada, N. Ono, *J. Appl. Phys.* **2006**, *100*, 034502.
- [26] P. B. Shea, L. R. Pattison, M. Kawano, C. Chen, J. Chen, P. Petroff, D. C. Martin, H. Yamada, N. Ono, J. Kanicki, *Synth. Met.* **2007**, *157*, 190.
- [27] P. B. Shea, H. Yamada, N. Ono, J. Kanicki, *Thin Solid Films* **2012**, *520*, 4031.
- [28] S. Aramaki, J. Mizuguchi, *Acta Cryst.* **2003**, *E59*, o1556.
- [29] Y. Zhao, Q. Wang, Q. Meng, D. Ding, H. Yang, G. Gao, D. Li, W. Zhu, H. Zhou, *Bioorg. Med. Chem.* **2012**, *20*, 1240.
- [30] ADF, *SCM, Theoretical Chemistry*, Vrije Universiteit, Amsterdam, The Netherlands **2023**.